Triadic Hopf-static structures in two-dimensional optical pattern formation

Yu. A. Logvin, B. A. Samson, A. A. Afanas'ev, A. M. Samson, and N. A. Loiko
Institute of Physics, Belarus Academy of Sciences, 70 F.Skaryna Avenue, Minsk 220072, Belarus
(Received 2 July 1996)

We describe a type of dissipative structure, namely, triadic Hopf-static patterns, which are in fact drifting spots in a rhombic or rhomboidal arrangement. They are generated by a resonant interaction between simultaneously unstable Hopf and static modes. We analyze triadic Hopf-static patterns in a nonlinear optical system consisting of a thin layer of two-level material and a feedback mirror with explicit inclusion of delay effects. [S1063-651X(96)50811-1]

PACS number(s): 05.70.Fh, 42.65.Sf, 47.54.+r

Spontaneous pattern formation in systems driven out of equilibrium becomes especially intricate when Hopf and static instabilities develop simultaneously. Such situations have been studied both theoretically and experimentally in chemical systems [1–3] as well as in hydrodynamics [4–6]. It was shown that a simultaneous excitation of Hopf and static modes can give rise to a coexistence of traveling and steady rolls (stripes) [5,2]. Another result was that spatially subharmonic oscillations generated by resonance interaction between the Hopf and static modes in one-dimensional (1D) systems might be accompanied by a spatiotemporal chaos [6,7].

In comparison with the 1D case, 2D geometry implies a richer variety of structures and a larger number of possible resonant combinations in the mode interaction. For example, in the case of an absence of the static instability, an interaction of Hopf modes results in a whole family of patterns including traveling and standing rolls, squares and rhombi, as demonstrated in a general treatment [8].

In this Rapid Communication, on a basis of concrete optical pattern-forming scheme, we report on stable 2D patterns, namely, drifting rhombic and rhomboidal structures produced by resonant interaction of the Hopf and static modes. Finding parallels with the resonant-triad nonlinear interaction in hydrodynamical boundary-layer transitions [9], we call the structures triadic Hopf-static patterns. The emergence of such a kind of pattern is natural for optics because of diffraction of light during its propagation with a finite velocity. Delay effects give rise to Hopf instabilities in lasers [10], passive ring cavities [11], and half cavities [12]; diffractional coupling is responsible for the formation of static patterns in many optical schemes, where delay effects are negligible [13].

Here we consider a single feedback mirror scheme, which in different modifications became very popular in studies of optical pattern formation [12,14–18] because of its relative simplicity. As shown in Fig. 1(a), a plane-wave light field with amplitude e_0 is incident on a thin layer of nonlinear material. After transmission through the layer, light is fed back by a mirror that is set parallel to the layer in distance d. Coupling between the transmitted field (amplitude e_t) and the reflected field (amplitude e_r) is given by the diffractional paraxial operator $\hat{F}$,

$$e_r(\mathbf{r}_\perp,t)=\hat{F}e_t(\mathbf{r}_\perp,t-\tau)\equiv e^{-i(d/k)\Delta_\perp}e_t(\mathbf{r}_\perp,t-\tau), \quad (1)$$

where k is the light wave number, $\Delta_\perp$ is the Laplacian over transverse coordinates $\mathbf{r}_\perp=\{x,y\}$, and τ is the time delay in the feedback loop. It is supposed that the mirror reflectivity is equal to unity and the distance d contains an integer number of half wavelengths.

As the nonlinear medium we assume a film of two-level centers with a thickness much less than the wavelength of incident light, which allows us to neglect light diffraction and delay inside the layer. The light-matter interaction is described in this case by the Bloch equations for normalized polarization r and population difference w:

$$r_t=(-1+i\delta)r+iew, \quad (2)$$

$$w_t=-\gamma(w+1)+i(e^*r-r^*e)/2, \quad (3)$$

where δ is the frequency detuning between the incident field and two-level transition, $\gamma=T_2/T_1$ is the ratio between the transversal and longitudinal relaxation times, and the expression for the field e driving the centers in the film is given by

$$e(\mathbf{r}_\perp,t)=e_0+e_r(\mathbf{r}_\perp,t)-i2Cr(\mathbf{r}_\perp,t). \quad (4)$$

It is seen that the total field in the film consists of two fields illuminating the layer from both sides, as well as of the superradiance field proportional to the polarization r with the constant C known as the bistability parameter [17]. In addition, the transmitted and external incident fields are related as

$$e_t(\mathbf{r}_\perp,t)=e_0-i2Cr(\mathbf{r}_\perp,t). \quad (5)$$

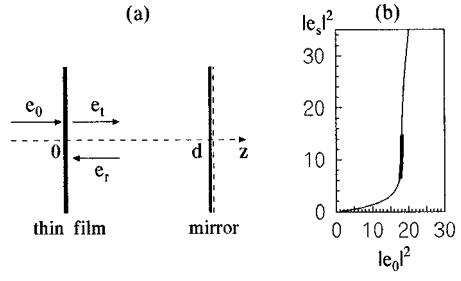

FIG. 1. (a) Single feedback mirror optical scheme. See the text. (b) Steady-state characteristic determined by Eq. (7) at $C=3.5$ and $\delta=-2$. The interval of instability is marked by the solid line.

In the limit of very long delay, when relaxation times are much shorter than the delay time τ, the time derivatives in Eqs. (2) and (3) can be omitted and the system is reduced to a nonlinear mapping, which takes the form

$$z_n = e_0 + \frac{2C(1+i\delta)(z_n+\hat{F}z_{n-1})}{(1+\delta^2)+|z_n+\hat{F}z_{n-1}|^2}, \tag{6}$$

where the transmitted field $[z_n(\mathbf{r}_\perp)\equiv e_t(\mathbf{r}_\perp, t=n\tau)]$ is chosen as a dynamical variable. Below we study both the continuous-time model and the mapping with a comparison of the results.

The homogeneous steady state is found through solution of a cubic equation for the field intensity inside the field $|e_s|^2$:

$$|e_0|^2 = |e_s|^2\left[\left(1+\frac{4C}{1+\delta^2+|e_s|^2}\right)^2+\left(\frac{4C\delta}{1+\delta^2+|e_s|^2}\right)^2\right]. \tag{7}$$

Depending on the parameters C and δ, the system can demonstrate optical bistability [17]. Here we choose parameters to work in the regime of nascent bistability [Fig. 1(b)].

Analyzing the stability of the steady state with respect to perturbations proportional to $\exp(\lambda t + i\mathbf{k}_\perp\mathbf{r}_\perp)$, we find the neutral stability curves determined by the quasipolynomial $D(\lambda)$. An expression for $D(\lambda)$ is cumbersome and is presented elsewhere [19]. We note only that due to diffractional coupling (1), $D(\lambda)$ depends on $\sin\theta$ and $\cos\theta$, where $\theta = k_\perp^2 d/k$. This periodicity on θ causes the occurrence of an infinite number of instability zones distinguished by the wave numbers of the structure to be developed. In Fig. 2 only the 2π interval is presented. We found two kinds of zones corresponding to Hopf $[\Omega\equiv \mathrm{Im}(\lambda)\neq 0]$ and static $(\Omega=0)$ instabilities. Figure 2(a) shows that at a short-time delay the static instability dominates. With increasing delay [Figs. 2(b) and 2(c)] the Hopf zones grow and tend to the size of the static zones, which are invariable at any delay. Due to the transcendental structure, the quasipolynomial $D(\lambda)$ has several roots, the number of which grows with increasing τ. A consequence of this can be seen in Fig. 3(c), where the secondary Hopf zones are dipped into the primary ones.

Studying the stability of complex mapping (7) yields a quadratic equation for the multiplicator Λ. The condition of stability is now $|\Lambda|<1$. Two domains in Fig. 2(d) are in agreement with the instability zones found in the continuous-time treatment in the limit $\tau\to\infty$. In the domain bounded by dashed line, $\Lambda<-1$ (Hopf type of instability), while another zone with $\Lambda>1$ corresponds to static instability.

Resuming the linear stability analysis, we note that at long delay, the development and resonance competition of several modes that are unstable due to both Hopf and static mechanisms should be anticipated, which is investigated below by means of the numerical simulations (details of the numerical scheme may be found in Ref. [17]). The results of the simulations can be classified as follows.

(i) At short delay that corresponds to Fig. 2(a), the static instability dominates and with increasing incident light intensity we observed the emergence of static patterns in the form of positive ($H0$) hexagons with their successive transformation to rolls and further to negative ($H\pi$) hexagons. Such a transition is a rather conventional phenomenon in the systems demonstrating a change in sign of the quadratic coupling responsible for hexagon formation [20,21,14,18].

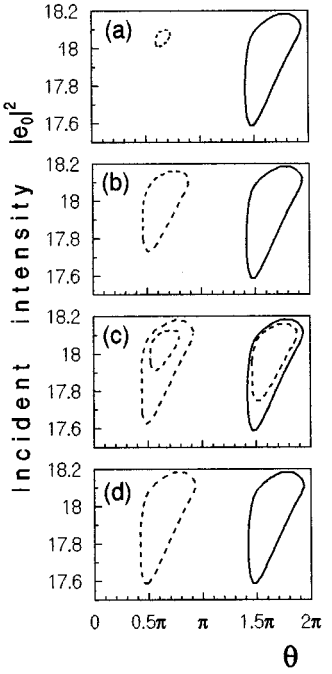

FIG. 2. Neutral stability curves for $C=3.5$, $\delta=-2$, and $\tau=5$ (a), 10 (b), and 15 (c) and for nonlinear mapping (d). Solid (dashed) curves correspond static (Hopf) instabilities.

(ii) At relatively long delay ($\tau>12$), we observed a development of Hopf modes and their competition with the static ones. We used the filtering in $\mathbf{k}_\perp$ space to ''cut off'' the static balloon at $\theta>\pi$ and to make the situation clear for purely Hopf bifurcation. In this case, using different initial

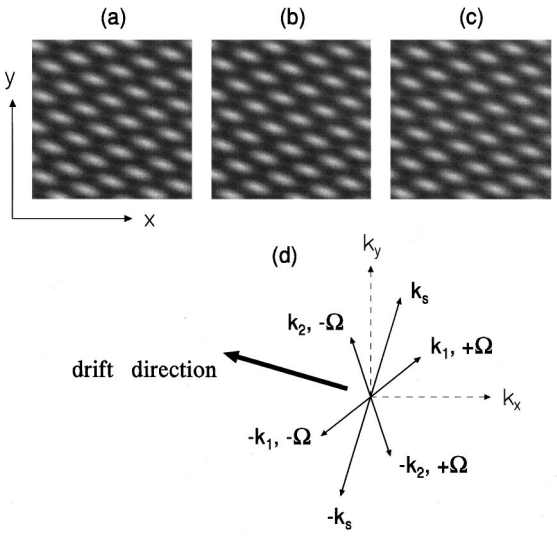

FIG. 3. Snapshots of drifting triadic Hopf-static pattern obtained from the continuous-time model at three successive moments of time for the parameters of Fig. 2(c) and $|e_0|^2=17.8$. (d) illustrates the instantaneous 2D Fourier spectrum.

conditions, we obtained structures permitted by the symmetry rules for the Hopf bifurcation on a plane [8]: traveling and alternating rolls.

(iii) We studied the interaction between the Hopf and static modes, with the result described below.

Starting the simulation of the continuous-time model near the lower threshold of the instability interval of Fig. 1(b), we observed the emergence of a moving pattern with a rhombic symmetry. In Figs. 3(a)–(c) the snapshots of the light intensity inside the film at three successive moments of time are shown. The instantaneous 2D spatial Fourier spectrum in Fig. 3(d) witnesses that two pairs $\pm\mathbf{k}_1$ and $\pm\mathbf{k}_2$, as a result of composition, give a third pair $\pm\mathbf{k}_s=\pm\mathbf{k}_1\pm\mathbf{k}_2$. A comparison of the vector moduli with the results of the linear stability analysis in Fig. 2 shows that $\pm\mathbf{k}_1$ and $\pm\mathbf{k}_2$ belong to the Hopf instability band, whereas $\pm\mathbf{k}_s$ corresponds to the static structure. Therefore, we call the observed structures triadic Hopf-static (THS) patterns. One can see from Figs. 3(a)–(c) that the structure performs a drifting motion in the direction indicated by the bold arrow in Fig. 3(d). Pattern dynamics becomes more obvious if we express the light intensity in the film as

$$I=I_{\mathrm{bias}}+\frac{1}{2}Se^{i\mathbf{k}_s\cdot\mathbf{r}_\perp}+\frac{1}{2}H_1e^{i\mathbf{k}_1\cdot\mathbf{r}_\perp+i\Omega t}+\frac{1}{2}H_2e^{i\mathbf{k}_2\cdot\mathbf{r}_\perp-i\Omega t}+\mathrm{c.c.}, \tag{8}$$

where S and $H_{1,2}$ are complex amplitudes of the static and Hopf components, respectively. Supposing for the moment the amplitudes to be real and $H_1=H_2\equiv H$, we can reduce Eq. (8) to

$$I=I_{\mathrm{bias}}+S\cos(\mathbf{k}_s\cdot\mathbf{r}_\perp)+2H\cos\left(\frac{\mathbf{k}_1+\mathbf{k}_2}{2}\cdot\mathbf{r}_\perp\right)\cos\left(\frac{\mathbf{k}_1-\mathbf{k}_2}{2}\cdot\mathbf{r}_\perp-\Omega t\right), \tag{9}$$

where the last term indicates motion of the pattern with a velocity $v=2\Omega/|\mathbf{k}_1-\mathbf{k}_2|$. Obviously, the direction of the motion is determined by the initial conditions. Note that in the process of motion the structure reproduced itself with a period $2\pi/\Omega$, which tends to 2τ for long τ. With increased incident light intensity $I_0\equiv|e_0|^2$, we observed a transition to the stripes moving in a direction set by the one of the Hopf modes. Near the opposite edge of the instability interval the THS patterns were found again. The only difference from those presented in Fig. 3 was the inverse contrast.

Simulations with the mapping confirmed results of the continuous-time treatment. With increased I_0 we observed an emergence of positive THS structures with pulsation period being two iterations. The top and bottom pictures in Fig. 4(a) show the corresponding established structures at two successive iterations. With a further increase of I_0 we saw a transition to the pulsating stripes [Fig. 4(b)]; the negative THS structures were found [see Fig. 4(c)] near the upper threshold.

Starting the simulations of the mapping with another set of initial conditions, we got the THS structures of rhomboid symmetry (Fig. 5). Here the H_1 and S modes belong to the instability balloons shown in Fig. 2 within $0<\theta<\pi$ and

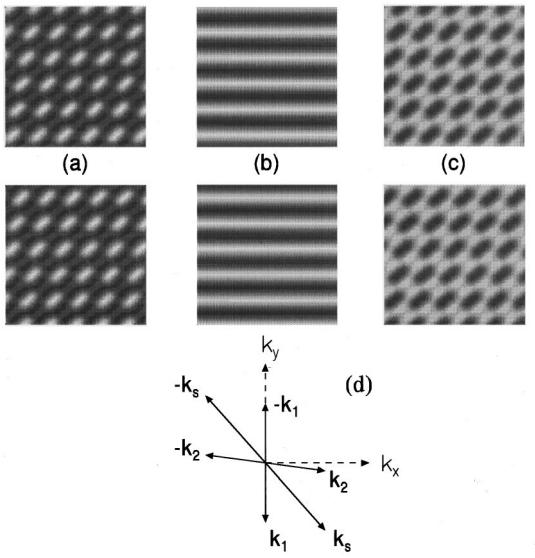

FIG. 4. Positive THS patterns [(a), top and bottom] obtained from the mapping (6) at two successive iterations for the parameters $C=3.5$, $\delta=-2$, and $|e_0|^2=17.8$, stripes at $|e_0|^2=18.0$ (b), negative THS patterns at $|e_0|^2=18.05$ (c), and 2D spatial wave vectors for the THS pattern (d).

$\pi<\theta<2\pi$ intervals, respectively, while the H_2 mode lies within $2\pi<\theta<3\pi$. Now, the Hopf modes have different wave numbers [the corresponding $k_\perp$ diagram is shown in Fig. 5(d)]. With increasing I_0 we observed the transition from positive THS structures [Fig. 5(a)] with the pulsation period being two iterations to the stationary stripes [Fig. 5(b)] produced by the S mode. Figure 5(c) presents the negative THS patterns near the opposite edge of the instability interval. Note that similar THS patterns of rhomboidal symmetry were also found in simulations of the continuous-time model.

The whole scenario is quite remniscent of the transition from positive to negative hexagons, described in our item (i) and in Refs. [21,20,18]. Similarly to the static hexagons, here

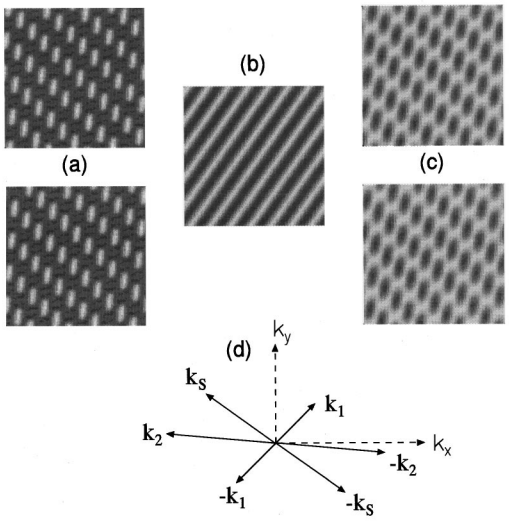

FIG. 5. Pattern sequence obtained from the mapping at the same parameters as in Fig. 4 with the only difference being the initial conditions.

the sum of the phases of the triad $\arg(S)+\arg(H_1)+\arg(H_2)$ is a main characteristic. For the structures near the lower and the upper edges of the instability interval in Fig. 1(b), this sum is equal to 0 and π, respectively. Therefore, we refer to the scenario described as a transition from positive to negative THS patterns through stripes.

An explanation of the scenarios described above may be given in terms of amplitudes equations that can be derived in the vicinity of the lower (upper) static mode excitation threshold. The threshold, for the Hopf mode, must be close to the static one in the case of a sufficient delay. Then, introducing the delay operator $\hat{D}=\exp[-\tau(d/dt)]$ and supposing $\tau\propto\varepsilon^{-1}$, where ε is, in fact, the distance from the threshold, which sets the scale for the standard multiple-scale expansion, the equations for three THS amplitudes are obtained. In a normalized form for the case of $\delta=0$ they read (cf. [7])

$$\frac{d}{dt}S=\varepsilon S+\sigma H_1H_2-[|S|^2+2\gamma(|H_1|^2+|H_2|^2)]S,$$

$$\frac{d}{dt}H_{1,2}=(\varepsilon-\Delta+i\Omega')H_{1,2}+(\sigma+i\sigma')H_{2,1}^{*}S-[|H_{1,2}|^2+2\gamma(|S|^2+|H_{2,1}|^2)]H_{1,2}, \quad (10)$$

where $\Delta\propto\Omega^2$ is the gap between thresholds for the static and Hopf modes, $\sigma=1$ at the lower threshold, and $\sigma=-1$ at the upper one. The imaginary coefficients $\Omega',\sigma'\propto\Omega$ may be skipped because they only renormalize the Hopf frequency value. It is easy to see that in a mapping limit $\tau\to\infty$, or $\Omega\to 0$, the Ginzburg-Landau equations (10) become identical to the amplitude equations for static hexagons [22]. Analogous to the case of hexagons, positive THS patterns occur at $\sigma=1$ and negative ones at $\sigma=-1$.

In conclusion, we described a class of 2D dissipative structures that arise as a result of development and resonant interaction of two Hopf and single static modes. Although the THS patterns are shown to emerge in the nonlinear optical system with delay, they should be inherent in other 2D pattern-forming systems permitting a resonance interaction of the Hopf and static modes.

[1] H. Kidachi, Prog. Theor. Phys. **63**, 1152 (1980).

[2] J.-J. Perraud, A. De Wit, E. Dulos, P. De Kepper, G. Dewel, and P. Borckmans, Phys. Rev. Lett. **71**, 1272 (1993).

[3] A. De Wit, G. Dewel, and P. Borckmans, Phys. Rev. E **48**, R4191 (1993).

[4] B.J.A. Zielinska, D. Mukamel, and V. Steinberg, Phys. Rev. A **33**, 1454 (1986).

[5] P. Kolodner, Phys. Rev. E **48**, R665 (1993).

[6] D.P. Vallette, W.S. Edwards, and J.P. Gollub, Phys. Rev. E **49**, R4783 (1994).

[7] D. Lima, A. De Wit, G. Dewel, and P. Borckmans, Phys. Rev. E **53**, R1305 (1996).

[8] M. Silber and E. Knobloch, Nonlinearity **4**, 1063 (1991); M. Silber, H. Riecke, and L. Kramer, Physica D **61**, 260 (1992).

[9] A.D.D. Craik, J. Fluid Mech. **50**, 393 (1971); F.T. Smith and P.A. Stewart, *ibid.* **179**, 227 (1987).

[10] N.A. Loiko and A.M. Samson, Kvant. Elektron. (Moscow) **21**, 713 (1994) [Sov. J. Quantum Electron. **24**, 657 (1994)].

[11] K. Ikeda, H. Daido, and O. Akimoto, Phys. Rev. Lett. **45**, 709 (1980).

[12] W.J. Firth, J. Mod.Opt. **37**, 151 (1990); G. D'Alessandro and W.J. Firth, Phys. Rev. A **46**, 537 (1992).

[13] Chaos, Solitons and Fractals **4** 1251 (1994), special issue on nonlinear optical structures, patterns, chaos, edited by L.A. Lugiato.

[14] T. Ackemann, Yu.A. Logvin, A. Heuer, and W. Lange, Phys. Rev. Lett. **75**, 3450 (1995).

[15] S. Residori, P.L. Ramazza, E. Pampaloni, S. Boccaletti, and F.T. Arecchi, Phys. Rev. Lett. **76**, 1063 (1996).

[16] E.V. Degtiarev and M.A. Vorontsov, J. Mod. Opt. **43**, 93 (1996).

[17] A.A. Afanas'ev, Yu.A. Logvin, A.M. Samson, and B.A. Samson, Opt. Commun. **115**, 559 (1995).

[18] B.A. Samson, Yu.A. Logvin, and W.J. Firth (unpublished).

[19] N.A. Loiko, Yu.A. Logvin, and A.M. Samson, Opt. Commun. **124**, 383 (1996).

[20] M. Tlidi and P. Mandel, Chaos, Solitons and Fractals **4**, 1475 (1994).

[21] W.J. Firth and A.J. Scroggie, Europhys. Lett. **26**, 521 (1994).

[22] S. Ciliberto, P. Coullet, J. Lega, E. Pampaloni, and C. Perez-Garcia, Phys. Rev. Lett. **65**, 2370 (1990).